Journal of Power Sources 506 (2021) 230141

Contents lists available at ScienceDirect

Journal of Power Sources

journal homepage: www.elsevier.com/locate/jpowsour

Laminar burning velocity of gases vented from failed Li-ion batteries

M. Henriksen [a,*], K. Vaagsaether [a], J. Lundberg [a], S. Forseth [b], D. Bjerketvedt [a]

[a] Faculty of Technology, Natural Sciences and Maritime Sciences, University of South-Eastern Norway, Kjølnes Ring 56, Porsgrunn, 3901, Norway
[b] Norwegian Defence Research Establishment (FFI), Instituttveien 20, 2007, Kjeller, Norway

HIGHLIGHTS

- Different gas compositions vented from failed Li-ion batteries (LIBs) are investigated.
- Laminar burning velocities (LBVs) of multiple gases are determined experimentally.
- The obtained LBVs are compared with the LBVs predicted by reaction mechanisms.
- Ideal prediction models are identified based on the CO_2 content in gas mixtures.
- Generation of a simplified gas to resemble combustion properties of an actual LIB vent gas.

ARTICLE INFO

Keywords:
Li-ion explosion hazard
Combustion properties
Safety
Vented Li-ion gas
Laminar burning velocity
Reaction mechanisms

ABSTRACT

In the last decade, several fires and explosions caused by Li-ion batteries (LIBs) have been reported. This can be attributed to the thermal runaway and catastrophic failures of LIBs that release combustible gases, which when mixed with air can lead to explosions and fires. To address this explosion hazard, we determine the laminar burning velocity (LBV) of three gas compositions associated with Li-ion failure and a pseudo (simplified) gas in a 20-L explosion sphere at 300 K and 100 kPa. This simplified gas avoids toxic gases in experiments and represent the desired explosion characteristics. The LBVs in the case of gas compositions range from approximately 300 to 1050 mm s^{-1}. Additionally, four different reaction models are used to estimate the LBVs of these gas compositions. We compare the theoretical and experimental results to determine the prediction accuracy of the reaction models. All reaction models over- or under-predicted the LBV for the different gas compositions. A recommendation for choosing reaction models is given to predict LBV for various gas compositions. This study's results are intended as input to computational fluid dynamic simulations but can be used directly in safety engineering models.

1. 1. Introduction

The need for sustainable and emission-free energy has increased the demand for Li-ion batteries (LIBs) as leading energy storage units [1]. However, LIBs exhibit an inherent risk of catastrophic failures. Owing to the use of flammable organic electrolyte solvents and temperature-sensitive electrodes in Li-ion cells, a battery management system is required to ensure safe operation. A catastrophic failure or a thermal runaway may generate and release combustible gases and evaporate the electrolyte components. These combustible gases mixed with air can cause explosions and fires. Several severe accidents caused by failed LIBs have been reported in the last decade [2–6].

Numerous events, including heat exposure, mechanical abuse, overload, overcharge, under-discharge, and internal or external short circuits can lead to a catastrophic failure of an LIB. Any of these events can initiate self-heating that may result in thermal runaway [7]. Sufficient self-heating will cause the evaporation and decomposition of the electrolyte solvent, which increases the internal pressure. Consequently, the Li-ion cell may vent or rupture [5]. The gas released during venting or rupturing can be a mixture of hydrogen, carbon monoxide, carbon dioxide, and various hydrocarbons [8].

Since the early 2000s, several researchers have conducted experimental studies to explore the composition of gases released from failing LIBs. Certain studies focused on the toxic gases released during cell venting. For instance, Larsson et al. [9] and Nedjalkov et al. [10] reported a significant amount of a toxic substance, hydrogen fluoride.

* Corresponding author.
E-mail address: mathias.henriksen@usn.no (M. Henriksen).

https://doi.org/10.1016/j.jpowsour.2021.230141
Received 18 March 2021; Received in revised form 13 May 2021; Accepted 3 June 2021
Available online 10 June 2021

Moreover, Nedjalkov et al. identified five additional substances that cause acute toxicity. This study focuses on the combustible gases released during thermal abuse testing of commercial LIBs in an inert atmosphere. Table 1 list a few examples of experimental studies [11–14] which fit the mention criteria. The species concentrations in Table 1 are normalized so that the sum of each gas composition equals 100%. The different gas mixtures in Table 1 indicate that the composition depends on the state of charge (SOC) and cell type or chemistry. For a more compressive list of gas releases from cell failure and thermal runaway, we suggested the following articles by Baird et al. [4], Wang et al. [11], and Fernandes et al. [12].

Laminar burning velocity (LBV) is a fundamental property of combustion and an important parameter in understanding the flame propagation, gas explosions, and combustion reaction mechanisms [17–19]. The LBV is used as a parameter in computational fluid dynamic (CFD) simulations to model turbulent combustion in large-scale explosions [20] and safety engineering models. Baird et al. [4] studied the explosive limits and the LBV of several gas compositions vented from failing LIBs, including the mixtures presented in Table 1. The combustion properties were calculated using the open-source tool Cantera [21] and the GRI-MECH 3.0 [22] reaction mechanism. The experimental results indicated that the LBV of the mixtures were in the range between 0.4 and 1.1 m s^{-1} [4].

In this study, we investigated the LBV of three potential gases released during an LIB venting. Experimentally determine LBV of gases released from LIBs has not been previously published; at least we found no such publications. The scope of this study was limited to the most common flammable species shown in Table 1. Therefore, the influence of fluorinated species and electrolyte solvents was neglected. However, fluorinated species can affect the LBV, and the explosion characteristics, as Gao et al. [23] showed in their study on explosion suppression of hydrogen explosions.

Based on the results reported by Baird et al. [4], we investigated the gas mixtures representing the upper and lower ranges of the LBV. The gas composition vented from a Lithium-nickel-cobalt aluminum (NCA) and Lithium-iron-phosphate (LFP) with a 100 SOC reported by Lammer et al. [13] and Golubkov et al. [16] (Table 1) were used as the basis for upper and lower LBVs gas compositions, hereafter referred to as the *high LBV Li-ion gas* and *low LBV Li-ion gas*, respectively. The third mixture was determined through several experiments conducted in a pressure vessel by heating commercial cells with cathode chemistry based on Lithium-iron-phosphate (LFP) with 100% SOC in an inert atmosphere. A gas chromatograph with a mass spectrometer detector analyzed the gas composition vented from LIBs, hereafter referred to as the *generic Li-ion gas*. These experiments were conducted by a research partner as part of the Norwegian Centre for Environment-friendly Energy Research, MoZEES [24].

In addition to the three different gas mixtures released from Li-ion batteries, we generated a pseudo or simplified gas, wherein the combustion properties were similar to that of the generic Li-ion gas composition. When studying an explosion in large-scale experiments, simplified gas has several advantages. Owing to the reduced number of species in the gas composition, less equipment is required when mixing the gases onsite and the cost of ordering large volumes of unique gas blends is reduced. Moreover, different combustion properties can be analyzed by adjusting only the ratio between species. Furthermore, the elimination of toxic species, such as carbon monoxide, can improve safety significantly. In this study, we generated a simplified gas mixture comprising hydrogen and methane, wherein their volume fractions were balanced to exhibit combustion properties similar to that of the generic Li-ion gas composition. Table 2 presents all four gas compositions studied experimentally and compared with theoretical calculations.

All experiments were performed in a 20-L explosion sphere [17,18] at 300 K and 100 kPa. The experimental results were compared with the theoretical calculations obtained using the open-source tool Cantera (version 2.4) [21]. Four different reaction mechanisms, namely the GRI-MECH 3.0 [22], the San Diego Mech [25], and two DMC combustion mechanisms reported by Glaude et al. [26] and Sun et al. [27] were used for the theoretical calculations. The results in this study are indented as input parameters for CFD simulations and safety engineering models.

Table 2
Gas compositions of the three potential gases vented from a failing Li-ion battery and the generated simplified gas.

Fuel mixture	H_2 [%]	CO [%]	CO_2 [%]	CH_4 [%]	C_2H_4 [%]	C_2H_6 [%]
High LBV Li-ion gas	42.8	37.1	10.0	7.1	3.0	[−]
Low LBV Li-ion gas	29.5	9.0	48.4	5.6	7.0	0.5
Generic Li-ion gas	34.9	25.0	20.1	15.0	5.0	[−]
Simplified gas	35.0	[−]	[−]	65.0	[−]	[−]

Table 1
Collection of normalized gas compositions vented from Li-ion batteries and cells during thermal abuse testing. The details are obtained from the existing literature [13–16].

REF.	Cell Type	SOC [%]	H_2 [%]	CO [%]	CO_2 [%]	CH_4 [%]	C_2H_2 [%]	C_2H_4 [%]	C_2H_6 [%]	C_3H_6 [%]	C_3H_8 [%]	C_4+ [%]
[13]	NCA-32A[c]	100	16.0	58.4	20.4	2.5	0.2	2.4	0.1	[−]	[−]	[−]
[13]	NCA-35E[c]	100	35.7	44.0	14.5	3.6	0.1	2.0	0.1	[−]	[−]	[−]
[13]	NCA-MJ1[c]	100	43.1	37.1	9.8	7.0	0.2	2.7	0.1	[−]	[−]	[−]
[14]	LCO	50	30.7	3.6	32.0	5.7	[−]	5.5	2.7	8.1	0.7	11.1
[14]	LCO	100	27.5	22.7	29.8	6.3	[−]	2.2	1.2	4.5	0.3	5.6
[14]	LCO	150	29.6	24.4	20.8	8.2	[−]	10.7	1.3	0.0	2.5	2.5
[15]	LCO/NMC	100	30.0	27.6	24.9	8.6	[−]	7.7	1.2	[−]	[−]	[−]
[15]	NMC	100	30.8	13.0	41.2	6.8	[−]	8.2	0.0	[−]	[−]	[−]
[15]	LFP	100	30.9	4.8	53.1	4.1	[−]	6.8	0.3	[−]	[−]	[−]
[16]	NCA	0[a]	1.3	1.4	95.7	1.3	[−]	0.3	0.0	[−]	[−]	[−]
[16]	NCA	50	17.5	39.9	33.8	5.2	[−]	3.2	0.4	[−]	[−]	[−]
[16]	NCA	100[b]	25.7	44.7	19.9	7.1	[−]	2.1	0.4	[−]	[−]	[−]
[16]	LFP	0	2.7	1.8	93.4	0.7	[−]	0.7	0.7	[−]	[−]	[−]
[16]	LFP	50	20.8	4.8	66.2	1.6	[−]	6.6	0	[−]	[−]	[−]
[16]	LFP	100	29.4	9.1	48.3	5.4	[−]	7.2	0.5	[−]	[−]	[−]

[a] The value is an average of five tests with identical chemistry and SOC.

[b] The value is an average of three tests with identical chemistry and SOC.

[c] The three gas compositions of the NCA cell type presented by Lammer et al. [13] are from different manufactures.

2. Materials and methods

Fig. 1 illustrates the experimental setup used in the study. A detailed description of the experimental setup, procedure, and determination of LBV is published previously [28,29]. The internal volume of the explosion sphere is 20 L, and a temperature-controlled heating jacket surrounding the vessel regulates the inner ambient temperature. While two pressure sensors recorded the explosion pressure, a separate pressure sensor was used to record the ambient pressure in the vessel during filling. Moreover, the separated fuel and air inlets reduced uncertainties in fuel–air concentrations. A single high-voltage spark ignited the fuel–air mixture. The flame propagation was recorded using a high-speed camera operating at 20,000 frames per second (fps) and the shadowgraph imaging technique [30]. We analyzed each image using an in-house image-processing algorithm generated in Python (v3.6) to obtain the temporal evolution of the flame radius.

The planar unstretched LBV (S^0_u) was calculated based on the temporal evolution of the flame radius. A detailed description of the procedure is published previously [28,31]. The laminar flame speed (S^0_b) and the Markstein length (L_b) is curve fitted to the implicit functions of radii ($r(t)$), which are the derivatives obtained from the most common stretch extrapolation models [17]. A previous study [31] reported that the derivatives obtained from these stretch extrapolation models generate remarkably similar LBV. In this study, we present the LBV obtained from the linear stretch model as it is commonly used in literature. The equations presented below are used to calculate the laminar flame speed, the Markstein length, and the LBV. The maximum explosion pressure and the rate of explosion pressure rise were calculated based on the recorded pressure.

$$r_f(t) = S^0_b t - 2L_b \ln r_f + Cst \quad (1)$$

where, r_f, flame radius [m], S^0_b, laminar flame speed with respect to the burnt state [m s^{-1}], L_b, Markstein length with respect to the burnt state [m], Cst, integration constant [m]

$$S^0_u = S^0_b \frac{\rho_b}{\rho_u} \quad (2)$$

where, S^0_u, laminar burning velocity with respect to the unburnt state [m s^{-1}], S^0_b, laminar flame speed with respect to the burnt state [m s^{-1}], ρ_b, density with respect to the burnt state [kg m^{-3}], ρ_u, density with respect to the unburnt state [kg m^{-3}].

The Cantera module [21] comprises several routines and algorithms that aid in solving problems of thermodynamics, chemical kinetics, and transport processes. We used the *FreeFlame* algorithm that solves the governing equation of a steady laminar (planar) 1-D premixed adiabatic flame [32] to calculate the LBV. Furthermore, we used the thermodynamic solver *equilibrate,* which finds the composition with minimum Gibbs free energy at constant internal energy and volume, to calculate the constant-volume explosion pressure. Both calculations require a reaction model, which comprises the chemical kinetic, thermodynamic, and transport data of the included species and reactions, as input. The results obtained from four different reaction models were compared with the experimentally measured LBV.

The reaction models chosen in this study was GRI-Mech 3.0 [22], San Diego Mech [25], a reaction mechanism propose by Glaude et al. [26] and Sun et al. [27]. GRI-Mech 3.0, which is design for natural gas combustion, includes 53 species and 325 reactions. In the study by Baird et al. [4], GRI-Mech 3.0 was used exclusively to predict the combustion and explosion properties of gas vented from Li-ion cells. The San Diego reaction mechanism includes 57 species and 268 reactions and is design to suit a wide range of combustion processes. Both the reaction mechanism from Glaude et al. and Sun et al. (hereafter referred to as the Glaude model and Sun model, respectively) were designed to study DMC as an oxygenate additive in diesel combustion. The Glaude model contains 102 and 257 species, and the Sun model includes 802 and 1563 reactions. GRI-Mech 3.0 [22] and San Diego Mech [25] were chosen owing to their versatility in various combustion processes; whereas the Glaude model and the Sun model were selected because they include DMC. DMC is a commonly used electrolyte solvent that can be vented from failing LIBs [8,12].

The explosion characteristics of the simplified gas mixture were designed to resemble those of the generic Li-ion gas over a range of fuel–air equivalence ratios. Hydrogen (H_2) and methane (CH_4) were chosen as the simplified gas species owing to their high and low LBV and low and high constant volume explosion pressure, respectively. We determined the concentrations of H_2 and CH_4 in the simplified gas by matching its LBV and the explosion pressure to those of the generic Li-ion gas for a fuel–air equivalence ratio between 0.5 and 1.7. GRI-Mech 3.0 was used to calculate the combustion properties for both gas

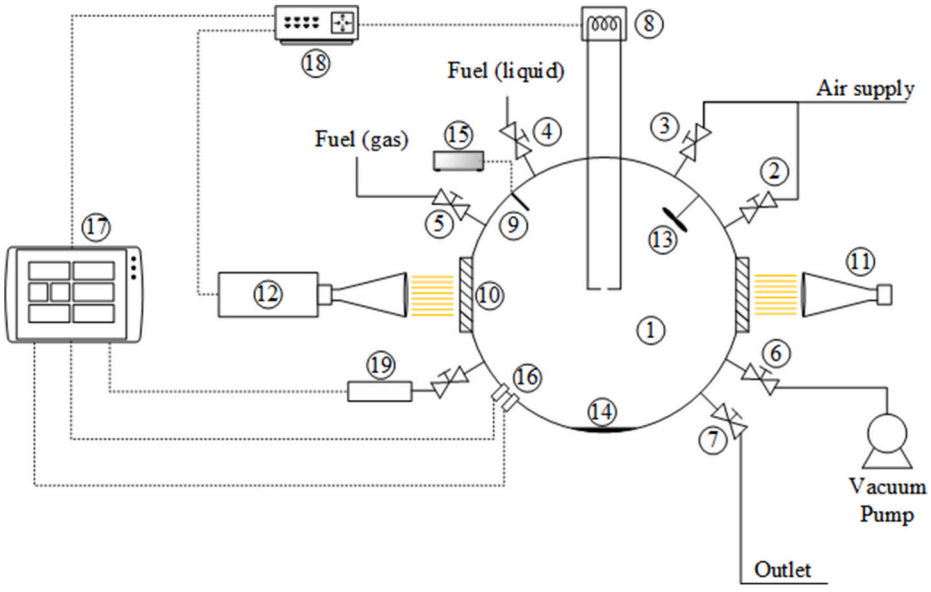

Fig. 1. Schematic of the experimental setup [28]. 1: explosion chamber; 2: oxidizer inlet; 3: flush inlet; 4: fuel (liquid) injection port; 5: fuel (gas) inlet; 6: vacuum port; 7: gas outlet; 8: ignition system; 9: thermocouple; 10: glass windows (100 mm); 11: LED light source; 12: high-speed camera; 13: stirrer; 14: heating plate; 15: ambient temperature display; 16: dual explosion pressure sensors; 17: data acquisition system; 18: control/trigger unit and 19: ambient pressure sensor.

mixtures. With a concentration of 35% and 65% of H_2 and CH_4, respectively, the simplified mixture matched the generic Li-ion gas reasonably. Fig. 2 depicts the calculated values of LBV and the closed volume explosion pressure in the generic Li-ion gas and the simplified mixture.

Further, the coefficient of determination (R^2) and the standard deviation of the error (SDE) were calculated to quantify the comparison of reaction mechanisms and the experimental result. These terms are commonly used in regression analysis to determine the "goodness of fit." Table 3 summarizes the variables and equations used to calculate R^2 and SDE.

2.1. 3. Results

Table 5 summarizes the averaged results of the high LBV Li-ion gas mixture. As predicted, the highest recorded values exist on the fuel-rich side, wherein the fuel–air equivalence ratio (φ) > 1. The highest value of LBV recorded at φ = 1.4 is 1055 mm s^{-1}. Furthermore, the maximum laminar flame speed is 7153 mm s^{-1} at φ = 1.30; and the maximum explosion pressure and the maximum rate of explosion pressure rise are 0.78 MPa and 82.88 MPa s^{-1}, respectively, at φ = 1.20. However, the maximum explosion pressure is nearly identical for φ = 1.10 and φ = 1.20, with a difference of 0.03 kPa.

Table 6 summarizes the averaged results of the low LBV Li-ion gas mixture. The highest laminar burning velocity and laminar flame speed recorded at φ = 1.10 are 351 mm s^{-1} and 2266 mm s^{-1}, respectively. Additionally, the maximum explosion pressure and the maximum rate of explosion pressure rise measured at φ = 1.0 are 0.72 MPa and 25.34 MPa s^{-1}, respectively. Moreover, an average difference of 4 kPa is observed in the maximum explosion pressure between φ = 1.00 and φ = 1.10.

Table 3
Description of variables and equations used to calculate the coefficient of determination (R^2) and the standard deviation of the error (SDE).

Description	Variable and Equation
Experimental data value	Y
Mean experimental data value	$\overline{Y}$
Value calculated from reaction mechanism	$\widehat{Y}$
Number of data points	n
Sum of squared errors	$SSE = \sum_i (Y_i - \widehat{Y}_i)^2$
Sum of squared residuals	$SSR = \sum_i (\widehat{Y}_i - \overline{Y})^2$
Coefficient of determination	$R^2 = \frac{SSR}{SSE + SSR}$
Standard deviation of the error	$SDE = \sqrt{\left(\frac{SSE}{n-2}\right)}$

Table 7 summarizes the averaged results calculated for the generic Li-ion gas mixture. Herein, the highest laminar burning velocity (482 mm s^{-1}) is recorded slightly on the fuel-rich side (φ = 1.10), which concurs well with the preliminary calculation (Fig. 2). The highest laminar burning velocity and laminar flame speed recorded at φ = 1.10 are 484 mm s^{-1} and 3343 mm s^{-1}, respectively. Furthermore, the maximum explosion pressure and maximum rate of explosion pressure rise are 0.75 MPa and 35.81 MPa s^{-1}, respectively, at φ = 1.00.

Table 8 summarizes the averaged results of the simplified gas mixture, wherein the highest laminar burning velocity and laminar flame speed recorded at φ = 1.10 are 506 mm s^{-1} and 3751 mm s^{-1},

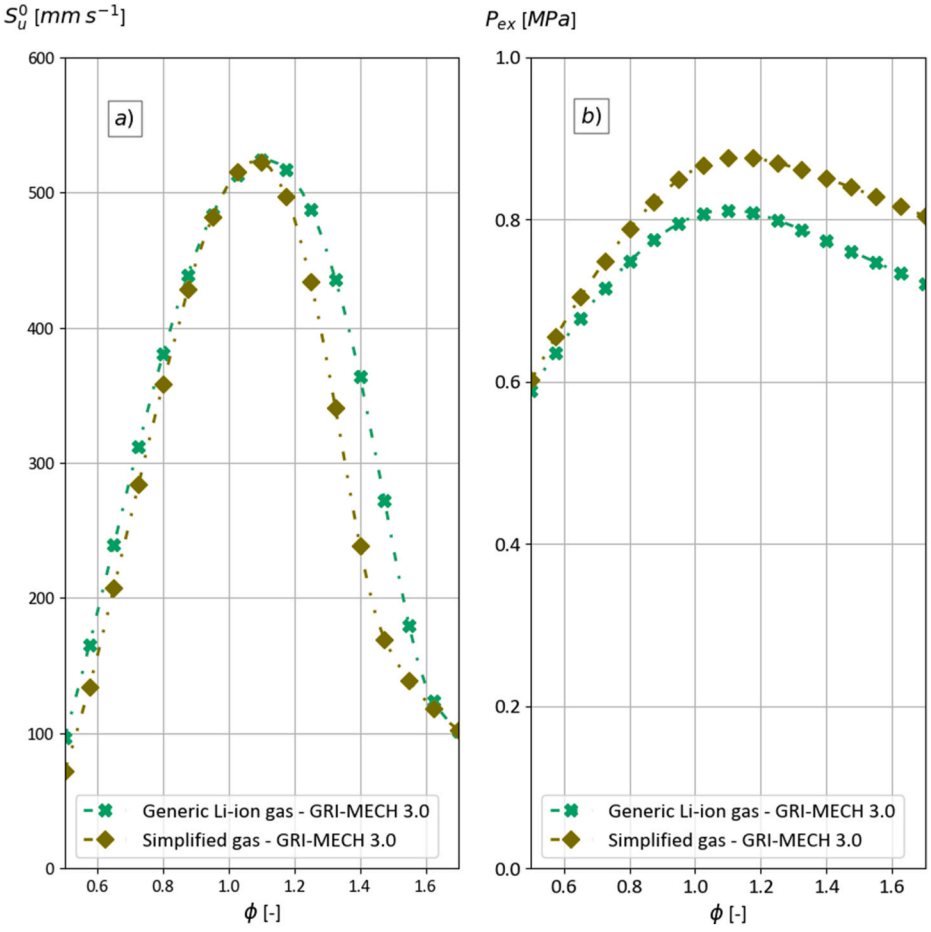

Fig. 2. Comparison of the calculated combustion properties of a generic Li-ion gas and the generated simplified gas. a): Comparison of the laminar burning velocity. b): Comparison of the explosion pressure.

Table 5
Laminar flame speed, Markstein length, laminar burning velocity, maximum explosion pressure, and maximum rate of explosion pressure rise measured for the high LBV Li-ion gas mixture at 300 K and 100 kPa absolute.

Fuel–air equivalence ratio	Laminar flame speed (S^o_b) [mm s^{-1}]	Markstein length (L_b) [mm]	Laminar burning velocity (S^o_u) [mm s^{-1}]	Maximum explosion pressure (P_{ex}) [MPa]	Maximum rate of explosion pressure rise $(dp/dt)_{ex}$ [MPa s^{-1}]
0.70	2939	−0.09	482	0.70	44.29
0.80	4071	0.21	627	0.74	59.81
0.90	5061	0.37	745	0.76	70.99
0.99	5965	0.46	852	0.77	77.15
1.10	6573	0.51	935	0.78	81.68
1.20	6984	0.52	1002	0.78	82.80
1.30	7152	0.52	1044	0.78	81.29
1.40	7101	0.53	1055	0.77	76.81

Table 6
Laminar flame speed, Markstein length, laminar burning velocity, maximum explosion pressure, and maximum rate of explosion pressure rise measured for the low LBV Li-ion gas mixture at 300 K and 100 kPa absolute.

Fuel–air equivalence ratio	Laminar flame speed (S^o_b) [mm s^{-1}]	Markstein length (L_b) [mm]	Laminar burning velocity (S^o_u) [mm s^{-1}]	Maximum explosion pressure (P_{ex}) [MPa]	Maximum rate of explosion pressure rise $(dp/dt)_{ex}$ [MPa s^{-1}]
0.80	1750	−0.31	292	0.67	21.26
0.90	2087	0.05	332	0.70	24.61
1.00	2256	0.12	347	0.71	25.10
1.10	2266	0.31	351	0.71	22.59
1.20	2087	0.44	333	0.69	18.18
1.30	1792	0.80	295	0.66	13.49

Table 7
Laminar flame speed, Markstein length, laminar burning velocity, maximum explosion pressure, and maximum rate of explosion pressure rise measured for the generic Li-ion gas mixture at 300 K and 100 kPa absolute.

Fuel–air equivalence ratio	Laminar flame speed (S^o_b) [mm s^{-1}]	Markstein length (L_b) [mm]	Laminar burning velocity (S^o_u) [mm s^{-1}]	Maximum explosion pressure (P_{ex}) [MPa]	Maximum rate of explosion pressure rise $(dp/dt)_{ex}$ [MPa s^{-1}]
0.70	1809	−0.36	306	0.66	22.00
0.80	2428	−0.09	384	0.70	29.40
0.90	2969	0.15	446	0.74	34.91
1.00	3308	0.31	479	0.75	35.79
1.10	3316	0.42	479	0.74	32.89
1.20	3051	0.61	451	0.74	27.66
1.30	2559	1.04	388	0.71	20.28
1.40	1900	2.19	295	0.68	11.69
1.50	1453	8.27	231	0.62	6.33
1.59	910	11.45	148	0.49	2.91

respectively. Additionally, the maximum explosion pressure recorded at $\varphi = 1.10$ (0.81 MPa) is only 1 kPa higher than that measured at $\varphi = 1.00$. The highest value of the maximum rate of explosion pressure rise recorded at $\varphi = 1.00$ is 39.66 MPa s^{-1}.

Table 9 presents the R^2 and SDE values determined using the experimental results and the theoretical calculations with the four reaction mechanisms using the equations in Table 3. The predictions of LBV by both GRI-Mech 3.0 and the Glaude model for the high LBV Li-ion concur well with the experimental results based on their calculated R^2 and SDE value. Moreover, the San Diego Mech and the Sun model obtained reasonable R^2 and SDE values, although they underestimate the LBV for $\varphi > 1.1$ (Fig. 3a).

Table 8
Laminar flame speed, Markstein length, laminar burning velocity, maximum explosion pressure, and maximum rate of explosion pressure rise calculated for the binary gas mixture at 300 K and 100 kPa absolute.

Fuel–air equivalence ratio	Laminar flame speed (S^o_b) [mm s^{-1}]	Markstein length (L_b) [mm]	Laminar burning velocity (S^o_u) [mm s^{-1}]	Maximum explosion pressure (P_{ex}) [MPa]	Maximum rate of explosion pressure rise $(dp/dt)_{ex}$ [MPa s^{-1}]
0.70	1623	−0.22	264	0.67	16.48
0.80	2450	−0.11	370	0.73	26.56
0.90	3223	0.27	455	0.78	35.05
1.00	3680	0.51	498	0.80	39.32
1.10	3751	0.55	506	0.81	37.60
1.20	3391	0.99	464	0.79	30.56
1.30	2636	1.80	369	0.76	19.26
1.38	1810	3.23	257	0.74	11.54
1.49	1194	8.58	174	0.62	5.35

Table 9
The calculated coefficient of determination (R^2) and standard deviation of the error (SDE) based on experimental laminar burning velocity (LBVs) and the LBVs predicted by the four different reaction mechanisms.

Fuel composition	GRI-Mech. 3.0	San Diego Mech	Glaude model	Sun model
	Coefficient of determination (R^2) [−]			
High LBV Li-ion gas	0.997	0.974	0.990	0.957
Low LBV Li-ion gas	0.547	0.720	0.585	0.970
Generic Li-ion gas	0.860	0.984	0.687	0.952
Simplified gas	0.990	0.972	0.772	0.950
	Standard deviation of the error (SDE) [mm s^{-1}]			
High LBV Li-ion gas	11.55	28.39	20.55	37.44
Low LBV Li-ion gas	60.96	20.42	38.93	4.50
Generic Li-ion gas	47.71	13.74	81.77	21.97
Simplified gas	12.09	19.94	78.89	26.15

Conversely, only the Sun model predicts LBVs that results in high R^2 and low SDE values for the low LBV Li-ion gas; the other three reaction mechanisms, particularly the GRI-Mech 3.0 and the Glaude model overestimate the LBV, as illustrated in Fig. 3b.

Furthermore, the LBV predictions of the San Diego Mech and Sun model concur well with the experimental results of the generic Li-ion gas. All reaction mechanisms predict the LBVs accurately when $\varphi < 1$; however, as φ increases, both the GRI-Mech 3.0 and Glaude model overpredict the LBV (Fig. 3c).

Finally, the LBV predictions of GRI-Mech 3.0 concur best with the experimental results of simplified gas based on the calculated R^2 and SDE values (Table 9). Additionally, both the San Diego Mech and Sun model predict the simplified mixture reasonably well, as presented in Table 9 and Fig. 3 d. However, the Glaude model overestimates the LBV in comparison with the experimental results when $\varphi > 0.9$.

2.2. 4. Discussion

3.1.1. 4.1 Experimental uncertainties and observations

Thermal diffusion, hydrodynamic instabilities, and buoyancy may influence the flame propagation, generating uncertainties in the measured LBV [17,18]. Although no hydrodynamic instabilities caused by pressure changes or buoyancy instabilities are observed in the

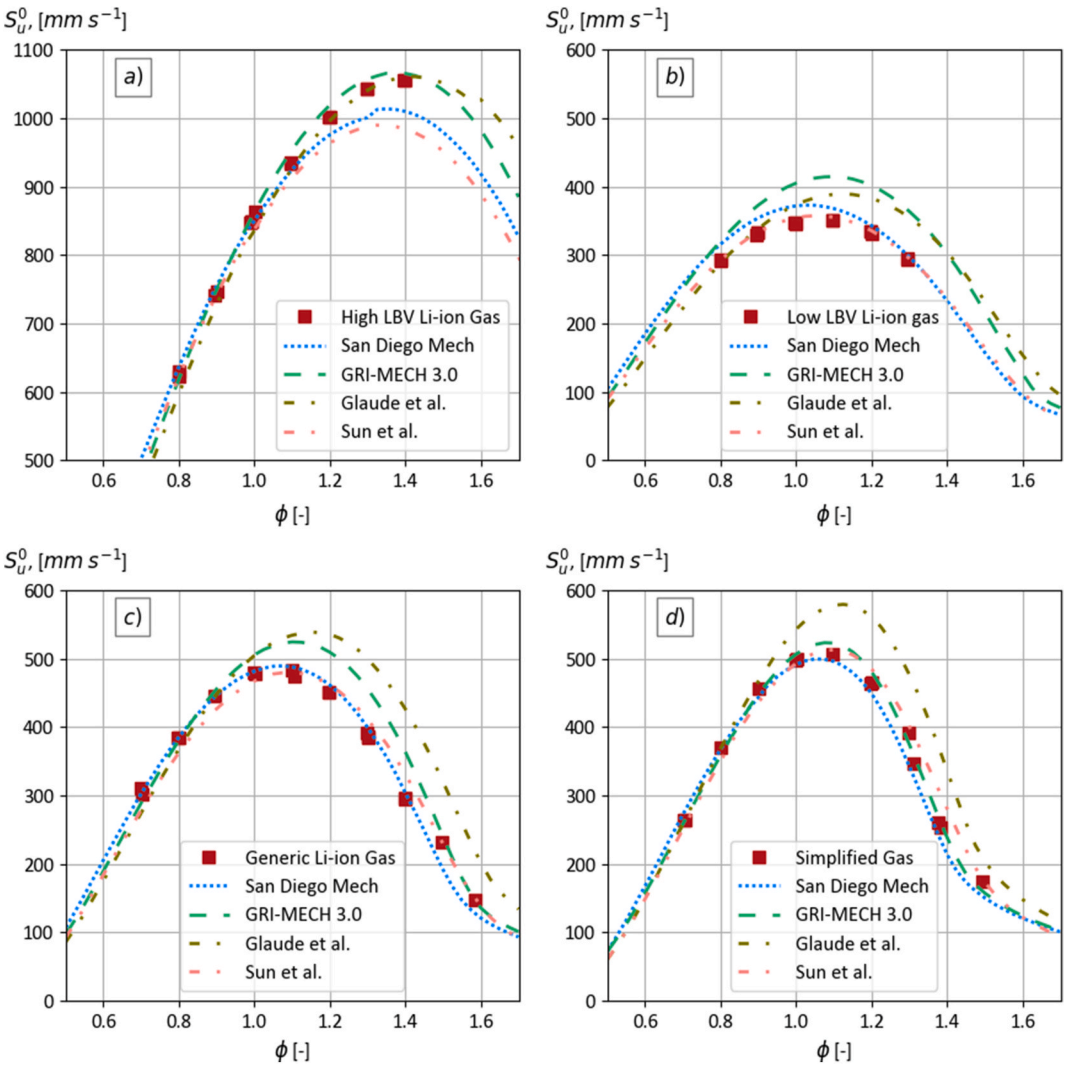

Fig. 3. Comparison of the predicted laminar burning velocity (LBV) using the four reaction mechanisms and the measured LBVs of a) the high LBV Li-ion gas mixture, b) the low LBV Li-ion gas mixture, c) the generic Li-ion gas mixture, and d) the simplified gas mixture.

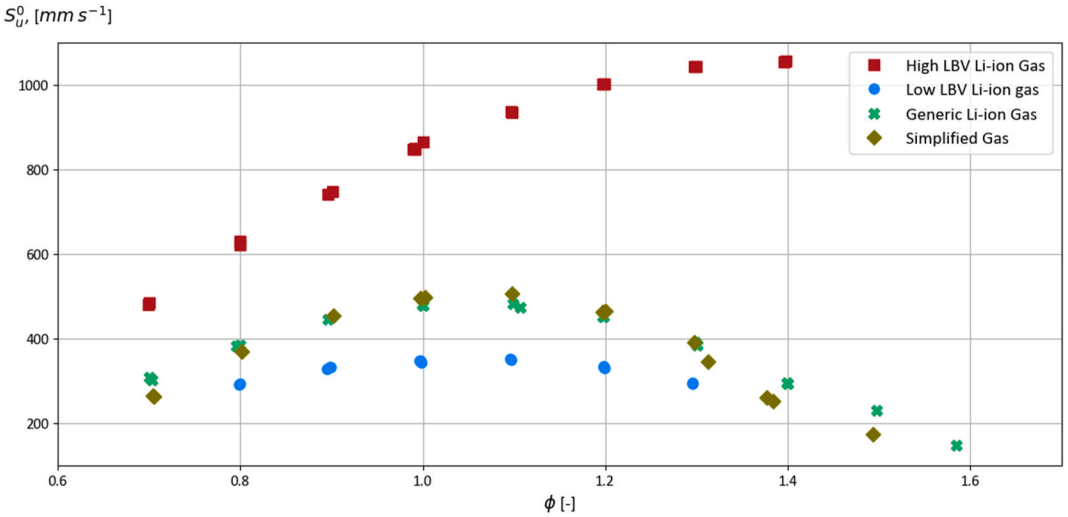

Fig. 4. Experimental laminar burning velocities obtained from four different gas compositions.

high-speed video of the experiments, minor front instabilities are observed in certain experiments on the far fuel-rich and fuel-lean sides. These can be attributed to thermal diffusion or ignition-induced instabilities. Moreover, the three mixtures with more than two species exhibited a higher tendency of front instabilities. Most of these front instabilities can be eliminated by adjusting the spark gap distance. However, the three gas compositions are significantly more sensitive to the spark gap distances than the simplified gas. To reduce the uncertainties, experiments with a flame front that does not propagate spherically are rejected. Moreover, parallel experiments are performed for nearly all concentrations to reduce the uncertainties in the experimental results further. However, only minor changes are observed in the LBV between two parallel experiments, as illustrated in Fig. 4.

The wide range of LBV observed between the gas compositions (Fig. 4) indicate that certain species influence the LBV significantly. The maximum LBV of the low LBV Li-ion gas is 351.4 mm s^{-1}, whereas that of the high LBV Li-ion gas is approximately three times higher at 1055.5 mm s^{-1}. Furthermore, pure H_2 has an LBV of approximately 2900 mm s^{-1} at a similar temperature and pressure [33,34]. The maximum LBV of a gas mixture with 5% H_2 and 95% CO is approximately 650 mm s^{-1} [35]. As the high LBV Li-ion gas comprises approximately 80% of H_2 and CO, a high LBV is expected. Additionally, CO_2 is an inert gas with a relatively high specific heat, which can reduce the amount of heat released from the combustible gas [36]. Consequently, an increase in the CO_2 concentration can lower the LBV. Therefore, as the low LBV Li-ion gas comprises approximately 50% CO_2, a low LBV is expected.

3.1.2. 4.2 LBV prediction accuracy of the reaction models

In this section, the LBV predictions of the four reaction models are compared to the experimentally obtained LBVs. A typical evaluation of reaction models is very compressive. The chemistry and reaction rates of gas mixtures must be analyzed [18,27]. In this study, however, we only perform a statistical analysis and compare the results with those reported in other similar studies to evaluate the LBV prediction accuracy of the reaction models.

A considerable discrepancy is observed in the prediction of the Glaude model in comparison with the experimental results. Except in the case of the experiment on the high LBV Li-ion gas, the Glaude model overestimates the LBV when $\varphi > 0.9$ in all other experiments. Additionally, previous studies have reported that the Glaude model deviates from experimentally obtained LBVs [27,31,37,38]. For instance, Bardin et al. [37] reported that the Glaude model over-predicts the LBV significantly in the case of methanol, ethanol, and DMC. Moreover, several studies [27,31,38] revealed similar results for the LBV of DMC. However, the Glaude model estimating the LBV of the high LBV Li-ion gas accurately (Fig. 3 and Table 9) could be attributed to the mixture composition, which primarily comprises H_2 and carbon monoxide (CO).

The GRI-Mech 3.0 model predicts the LBV for the high LBV Li-ion gas and simplified gas with the highest accuracy (Table 9 and Fig. 3). The high LBV Li-ion gas predominantly comprises H_2 and CO (approximately 80%), whereas the simplified gas comprises H_2 and CH_4 in the ratio of 35% and 65%, respectively. Although GRI-Mech 3.0 is developed for natural gas combustion, several experimental studies [35,39–41] reported that the model predicts the LBV for different syngas mixtures accurately. For instance, Wang et al. [35] reported that the GRI-Mech 3.0 predicts the LBV of gas mixtures comprising 95% CO and 5% H_2 with acceptable accuracy. Furthermore, the results of McLean et al. [41] on the LBV study of syngas mixture (50% CO and 50% H_2) are accurately predicted by the GRI-Mech 3.0 [22]. Both Rozenchan et al. [39] and Boushaki et al. [40] reported that the GRI-Mech 3.0 predicts the LBV for CH_4 accurately in several experiments under normal initial conditions. As the fuel composition of the high LBV Li-ion gas and the simplified gas are variations of the syngas and natural gas composition, respectively, the GRI-Mech 3.0 estimates the LBVs with an acceptable precision.

Conversely, the GRI-Mech 3.0 overestimates the LBVs of the low LBV Li-ion gas and the generic Li-ion gas. The discrepancy can be attributed to the higher CO_2 concentration as CO_2-rich mixtures exhibit higher heat loss owing to the thermal radiation. Typically, heat losses in a propagating flame reduce the propagation speed, which is not considered in the theoretical calculations, as it assumes adiabatic conditions. However, Yu et al. [42] studied the effect of thermal radiation on the LBV numerically and determined that the uncertainty is low, particularly for fuels diluted using species with strong radiative reabsorption properties. Thus, Yu et al. determined that the flame propagation speed increases when the fuel is diluted with up to 20% CO_2. Consequently, the increased radiative heat loss in the flame generated by the increased CO_2 is re-absorbed by the unburnt fuel. GRI-Mech 3.0 tends to over-predict the LBV as the CO_2 concentration increases in the fuel. Furthermore, Zahedi et al. [36] reported that the GRI-Mech 3.0 predicts slightly higher estimates of the LBV for 10% diluted CH_4 and 20% CO_2. Furthermore, the over-estimated LBVs in their study exists in a similar equivalence ratio range for the generic Li-ion gas with 20% CO_2.

Further, based on the R^2 values calculated using the San Diego Mech (Table 9), the model predictions concur well with the experimental results for all mixtures except the low LBV Li-ion mixture. Although the R^2 value is high for the high LBV Li-ion gas, Fig. 3 a) indicates that San Diego Mech under-estimates the LBV for $\varphi > 1.1$; the peak difference is 55 mm s^{-1} at $\varphi = 1.4$. By contrast, the peak difference between the LBV predicted by the San Diego Mech for the low LBV Li-ion gas and the experimentally obtained LBV is 25 mm s^{-1} with an R^2 value of 0.72. Additionally, the SDE (Table 9) determined indicates that the discrepancy between calculations and experimental results is large in the case of high LBV Li-ion gas than that of the low LBV Li-ion gas. Nilsson et al. [43] reported that the scatter between CH_4 LBV experiments is less than 20 mm s^{-1} based on the results observed over the last 15 years. Furthermore, the average deviance between the San Diego Mech predictions and the actual LBV of the low LBV Li-ion gas is 18 mm s^{-1}, which exists in the same range as the experimental uncertainty identified by Nilsson et al. Therefore, the San Diego Mech model designed to suit a broad range of combustion applications [25] ensures relatively reasonable predictions of the experimental LBV.

In comparison with the other reaction mechanisms, the Sun model is the most consistent with R^2 values, which are higher than 0.95 for all mixtures. However, similar to the San Diego model, the Sun model exhibits issues in predicting the LBV for high LBV Li-ion gas (Fig. 3a), wherein the largest deviance is 71 mm s^{-1} with average deviance of 27.4 mm s^{-1}. The reaction mechanism of the Sun model comprises 257 species and 1563 reactions, which renders this the most comprehensive model owing to the size. The second-largest reaction mechanism is the Glaude model with 102 species and 802 reactions. Typically, the computational time increases significantly owing to the detailed mechanism involved in the model despite higher prediction accuracy. Therefore, the Sun model requires 80 times longer computational time than the other reaction mechanisms.

An advantage of the Glaude and Sun models is that they contain the electrolyte solvent DMC. Although the studies in Table 1 do not report DMC or any other electrolyte solvent, a study by Roth et al. [8] reported 11.5% solvent in the vented gas from a failing LIB. Fernandes et al. [12] detected 42% DMC and 17% ethyl methyl carbonate (EMC) in the vented gas composition during overcharge abuse testing. These studies prove that electrolyte solvents, such as DMC can be present in the gases vented from an LIB. Furthermore, previous studies have reported that the Sun model predicts the LBV with high accuracy for pure DMC at normal conditions [31,38].

As shown, the different reaction models may yield different results when used to predict combustion properties intended for safety engineering models and as input to CFD. Although we identified certain discrepancies in LBV predictions, the uncertainties in models and CFD simulation can be substantially larger than the deviations between these reaction models.

3.1.3. 4.3 Ideal reaction mechanisms for different gas compositions

As indicated in Table 1, different SOC and chemistry can yield different gas compositions during an LIB failure. The experimental results (Fig. 3 and Table 9) verify that all reaction models over- or under-predict the LBV for the gas compositions listed in Table 2. Therefore, to predict the LBV accurately, we recommend selecting a reaction model based on the CO_2 concentration in the gas composition. Although the GRI-Mech 3.0 predicts the gas compositions with a low CO_2 concentration accurately, the LBV for gas compositions with 20% and higher CO_2 are over-predicted. Furthermore, both the San Diego Mech and Sun Model perform well in predicting the LBV for gas compositions with a CO_2 concentration above 20%. Based on the R^2 and SDE values (Table 9), we conclude that the San Diego Mech and Sun model perform better for gas composition with moderate and high concentrations of CO_2, respectively. Table 10 presents the method of choosing a reaction model to predict LBVs considering the CO_2 concentration in the gas compositions as a criterion. Fig. 5 illustrates the estimated LBVs for the different gas compositions (Tables 1 and 2) based on the details presented in Table 10. However, the criteria (Table 10) may be valid only for the gas compositions listed in Table 2. If a conservative estimation of LBVs is essential, GRI-Mech 3.0 can be considered as an ideal choice than the recommendations presented in Table 10.

The high and low LBV Li-ion gases are based upon cell type NCA-MJ1 [13] and one of the LFP batteries [16], respectively, with certain minor changes in the gas compositions. We remove the acetylene (C_2H_2) and ethane (C_2H_6) from the NCA-MJ1 owing to their low concentrations, and the other concentrations are adjusted accordingly. Fig. 5 illustrates a slight discrepancy between the NCA-MJ1 and the high LBV Li-ion gas owing to the lower H_2 concentration and the removed C_2H_2, which results in slightly lower LBV in the case of high LBV Li-ion gas. Conversely, the concentrations are reasonably identical (±0.2%) in the case of the compositions of low LBV Li-ion gas and the LFP, resulting in identical estimations of LBV (Fig. 5).

3.1.4. 4.4 Challenges in generating a simplified Li-ion gas

The simplified gas is generated based on the combustion properties calculated using the GRI-Mech 3.0. As presented in Fig. 3c) and Table 9, the GRI-Mech 3.0 do not predict the LBV for the generic Li-ion gas accurately. Based on these results, we conclude that both reaction mechanisms should have been used in the preliminary calculations; while the San Diego Mech is ideal for the generic Li-ion gas calculation, the GRI-Mech 3.0 can be used for the calculations of the simplified gas. These two mechanisms can predict the LBV with enhanced accuracy (Fig. 6).

However, despite the increase in the LBV prediction accuracy, the specie composition of the simplified gas will remain the same. This implies that if the LBV in simplified gas is lowered by reducing the H_2 concentration, the explosion pressure increases owing to the increase in CH_4, which further increases the discrepancy in closed volume explosion pressure. Moreover, the simplified gas can resemble the generic Li-ion gas to a certain extent using only two species. If a higher level of resemblance is required, a third inert component, such as CO_2 must be added. Additionally, the discrepancy between the calculated and the experimentally obtained explosion pressures can be attributed to the heat losses in the explosion sphere.

Table 10
Recommendation for choosing a reaction mechanism to predict laminar burning velocities of the gases vented from Li-ion batteries based on the carbon dioxide (CO_2) concentration in gas compositions.

Reaction mechanism	CO_2 concentration	Gas mixture
GRI-Mech 3.0	Less than 15%	Simplified, High LBV
San Diego Mech	Between 15% and 40%	Generic
Sun model	Above 40%	Low LBV

The simplified gas generated resembles the generic Li-ion gas only in terms of combustion properties. In actual experiments, gas dispersion and mixing with air are essential factors. For instance, the flow in the gravity current relies on the density difference [44]. The simplified gas and the generic Li-ion gas have a density of 0.45 kg m^{-3} and 0.86 kg m^{-3}, respectively, at 300 K and 100 kPa. As the simplified gas is lighter than the generic Li-ion gas, the dispersion will differ. However, the temperature of the gas released from a failing Li-ion battery is expected to be higher than 300 K. An increase in temperature reduces the density of the vented gas. Consequently, the combustion properties of the gas are altered. Therefore, matching both density and combustion properties of a vented Li-ion gas requires the knowledge of release temperature and species composition. Based on the results of this study, a non-toxic "pseudo" or "simplified" gas that reproduces the required properties can be designed using theoretical calculations.

4.0 5. Conclusions

To evaluate the explosion hazards related to gas vented from failed LIBs, we determined the Markstein length, laminar flame speed, LBV, maximum explosion pressure, and maximum rate of explosion pressure rise for various concentrations of three gas compositions and one pseudo (simplified) Li-ion gas. The high LBV Li-ion gas exhibited the highest measured LBV of 1055 mm s^{-1} owing to the high content of hydrogen and carbon monoxide. Conversely, the low LBV Li-ion gas comprised more than 50% carbon dioxide, which significantly decreased the LBV; the maximum measured LBV for the low LBV Li-ion gas was 351 mm s^{-1}. The experimental results are considered novel and can be used in risk assessments of battery installations.

The measured LBV was compared with the predictions of four reaction mechanisms, namely the GRI-Mech 3.0, San Diego Mech, Glaude model, and Sun model. Among these, the Sun model exhibited the highest coefficient of determination (R^2) based on the measured LBVs. However, in comparison with the other models, the highest discrepancy in the LBV prediction of high LBV Li-ion gas was observed in the Sun model, wherein the value was under-predicted by 71 mm s^{-1}. The GRI-Mech 3.0 predicted the LBV with the highest accuracy for gas compositions with low CO_2 content. However, when the CO_2 content was more than 20%, the GRI-Mech 3.0 over-predicted the LBV. Furthermore, the Sun model and San Diego Mech exhibited the most accurate predictions of the LBV when the CO_2 concentrations were moderate and high, respectively. Therefore, based on the CO_2 concentration in a Li-ion gas release, the ideal reaction mechanism can be selected to predict LBVs.

The simplified gas composition was designed with combustion properties similar to that of a generic Li-ion gas. To reduce the number of species and eliminate toxic species, such as carbon monoxide, the simplified gas comprised 65% hydrogen and 35% methane. The initial calculations indicated that the LBV was nearly identical when applying the GRI-Mech 3.0 reaction model. However, the experimentally determined LBV was slightly higher in the simplified gas than that of the original generic Li-ion gas. Although, altering the simplified specie composition would not improve the combustion property resembles. This is because matching both explosion pressure and LBV was challenging based on only hydrogen and methane. However, introducing a third inert species, such as carbon dioxide, will result in nearly equal numerical results in terms of explosion pressure and LBV. Thus, a simplified gas composition can be generated conveniently using tools (Cantera) to reproduce the combustion properties of a gas vented from failed Li-ion batteries. The elimination of toxic species in the combustible gas composition, such as carbon monoxide, can improve the safety of experiments significantly.

5.0. Glossary

Laminar burning velocity is one of the most fundamental properties in premixed combustion is the and gives an insight into the distinctive

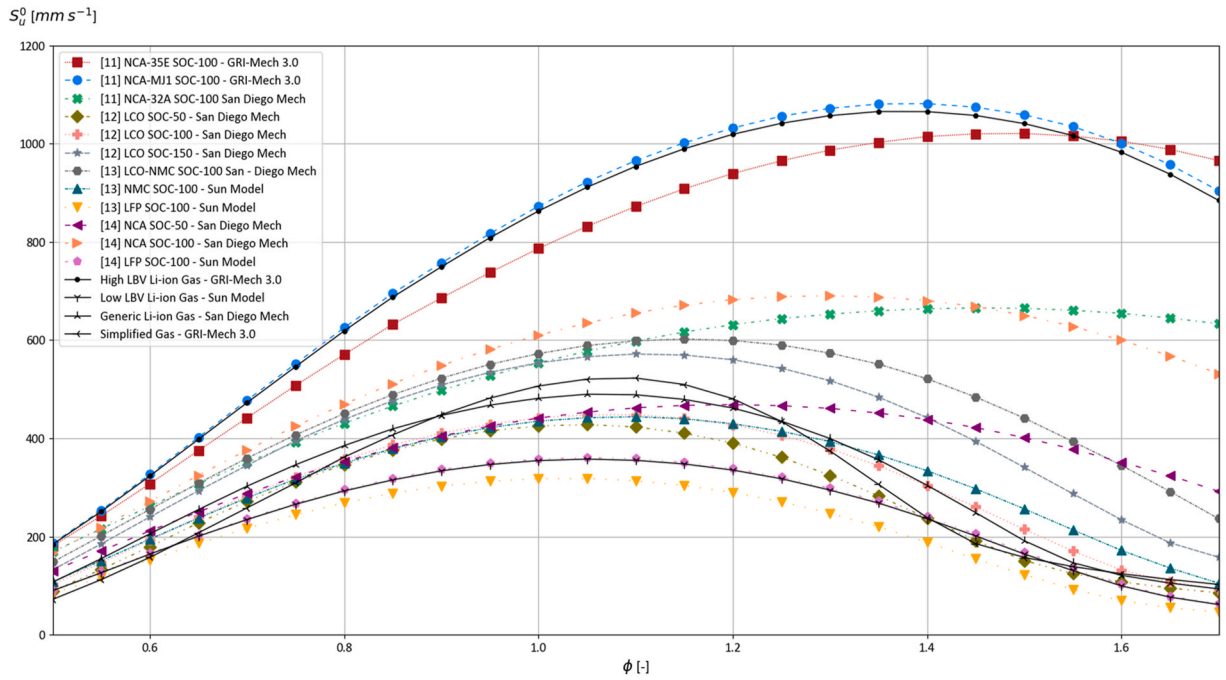

Fig. 5. Calculated laminar burning velocity for a collection of normalized gas compositions vented from Li-ion batteries during thermal abuse testing [11–14].

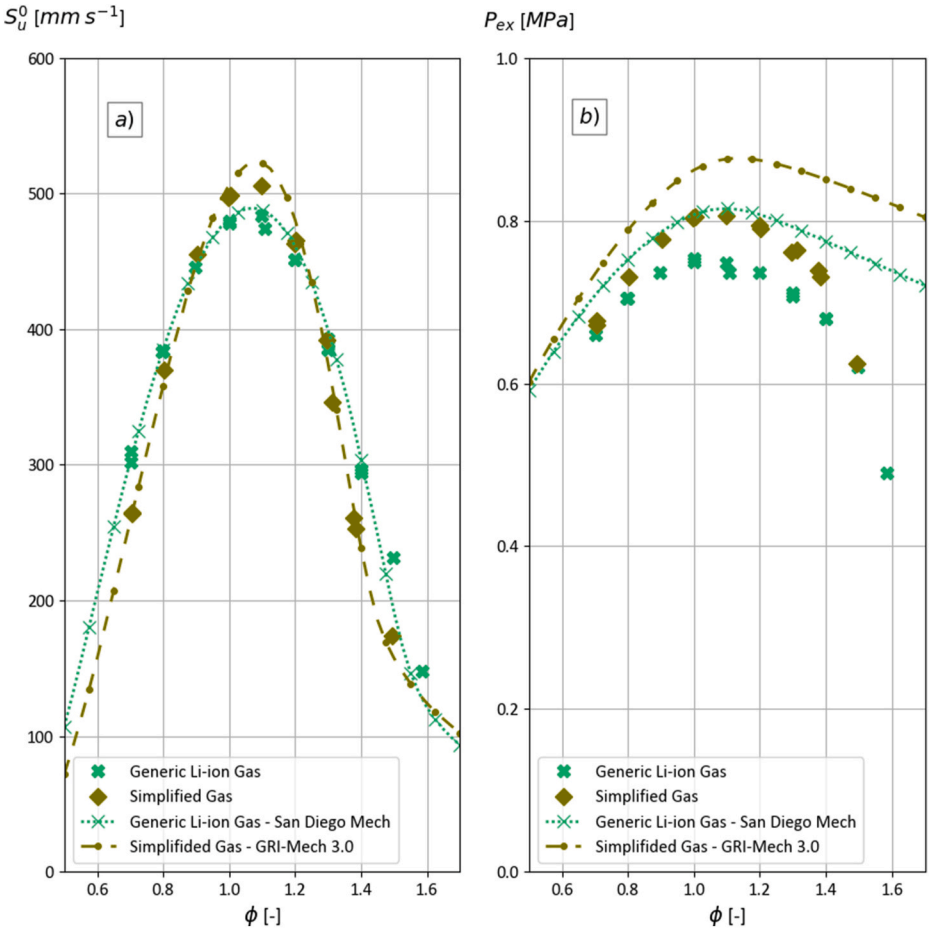

Fig. 6. Comparison of the generic Li-ion gas and the simplified gas based on experimental results, a) comparison of the laminar burning velocity, b) comparison of the close volume explosion pressure.

property of reactivity, exothermicity and in a given diffusive medium. It is defined as a planar/unstretched, adiabatic, one-dimensional velocity relative to the unburnt reactants [45].

Markstein length is a coefficient on which the effect of flame stretch/curvature has on the flame speed.

CRediT authorship contribution statement

M. Henriksen: Conceptualization, Methodology, Formal analysis, Writing – original draft, Writing – review & editing. **K. Vaagsaether:** Conceptualization, Methodology, Formal analysis, Writing – review & editing, Supervision, Funding acquisition. **J. Lundberg:** Conceptualization, Methodology, Formal analysis, Writing – review & editing, Supervision, Funding acquisition. **S. Forseth:** Formal analysis, Conceptualization, Writing – review & editing, Supervision, Funding acquisition. **D. Bjerketvedt:** Conceptualization, Methodology, Formal analysis, Writing – review & editing, Supervision, Funding acquisition.

Declaration of competing interest

The authors declare that they have no known competing financial interests or personal relationships that could have appeared to influence the work reported in this paper.

Acknowledgment

This work was performed within MoZEES, a Norwegian Centre for Environment-friendly Energy Research (FME). This work was supported by the Research Council of Norway [project number 257653]; and co-sponsored by 40 partners from the research industry and public sector.

References

[1] A. Mayyas, D. Steward, M. Mann, The case for recycling: overview and challenges in the material supply chain for automotive li-ion batteries, Sustain. Mater. Technol. 19 (2019), e00087, https://doi.org/10.1016/j.susmat.2018.e00087.
[2] D. Lisbona, T. Snee, A review of hazards associated with primary lithium and lithium-ion batteries, Process Saf. Environ. Protect. 89 (2011) 434–442, https://doi.org/10.1016/j.psep.2011.06.022.
[3] P.G. Balakrishnan, R. Ramesh, T. Prem Kumar, Safety mechanisms in lithium-ion batteries, J. Power Sources 155 (2006) 401–414, https://doi.org/10.1016/j.jpowsour.2005.12.002.
[4] A.R. Baird, E.J. Archibald, K.C. Marr, O.A. Ezekoye, Explosion hazards from lithium-ion battery vent gas, J. Power Sources 446 (2020) 227257, https://doi.org/10.1016/j.jpowsour.2019.227257.
[5] C. Mikolajczak, M. Kahn, K. White, R.T. Long, Lithium-Ion Batteries Hazard and Use Assessment, Springer US, Boston, MA, 2011, https://doi.org/10.1007/978-1-4614-3486-3.
[6] Q. Wang, P. Ping, X. Zhao, G. Chu, J. Sun, C. Chen, Thermal runaway caused fire and explosion of lithium ion battery, J. Power Sources 208 (2012) 210–224, https://doi.org/10.1016/j.jpowsour.2012.02.038.
[7] T. Lian, P.J.S. Vie, M. Gilljam, S. Forseth, Changes in thermal stability of cyclic aged commercial lithium-ion cells, ECS Trans 89 (2019) 73–81, https://doi.org/10.1149/08901.0073ecst.
[8] E.P. Roth, C.C. Crafts, D.H. Doughty, James McBreen, Advanced technology development program for lithium-ion batteries : thermal abuse performance of 18650 Li-ion cells. https://doi.org/10.2172/918751, 2004.
[9] F. Larsson, P. Andersson, P. Blomqvist, B.-E. Mellander, Toxic fluoride gas emissions from lithium-ion battery fires, Sci. Rep. 7 (2017), https://doi.org/10.1038/s41598-017-09784-z.
[10] A. Nedjalkov, J. Meyer, M. Köhring, A. Doering, M. Angelmahr, S. Dahle, A. Sander, A. Fischer, W. Schade, Toxic gas emissions from damaged lithium ion batteries—analysis and safety enhancement solution, Batteries 2 (2016) 5, https://doi.org/10.3390/batteries2010005.
[11] Q. Wang, B. Mao, S.I. Stoliarov, J. Sun, A review of lithium ion battery failure mechanisms and fire prevention strategies, Prog. Energy Combust. Sci. 73 (2019) 95–131, https://doi.org/10.1016/j.pecs.2019.03.002.
[12] Y. Fernandes, A. Bry, S. de Persis, Identification and quantification of gases emitted during abuse tests by overcharge of a commercial Li-ion battery, J. Power Sources 389 (2018) 106–119, https://doi.org/10.1016/j.jpowsour.2018.03.034.
[13] M. Lammer, A. Königseder, V. Hacker, Holistic methodology for characterisation of the thermally induced failure of commercially available 18650 lithium ion cells, RSC Adv. 7 (2017) 24425–24429, https://doi.org/10.1039/C7RA02635H.
[14] V. Somandepalli, K. Marr, Q. Horn, Quantification of combustion hazards of thermal runaway failures in lithium-ion batteries, SAE Int. J. Altern. Powertrains. 3 (2014) 98–104, https://doi.org/10.4271/2014-01-1857.
[15] A.W. Golubkov, D. Fuchs, J. Wagner, H. Wiltsche, C. Stangl, G. Fauler, G. Voitic, A. Thaler, V. Hacker, Thermal-runaway experiments on consumer Li-ion batteries with metal-oxide and olivin-type cathodes, RSC Adv. 4 (2014) 3633–3642, https://doi.org/10.1039/C3RA45748F.
[16] A.W. Golubkov, S. Scheikl, R. Planteu, G. Voitic, H. Wiltsche, C. Stangl, G. Fauler, A. Thaler, V. Hacker, Thermal runaway of commercial 18650 Li-ion batteries with LFP and NCA cathodes – impact of state of charge and overcharge, RSC Adv. 5 (2015) 57171–57186, https://doi.org/10.1039/C5RA05897J.
[17] A.A. Konnov, A. Mohammad, V.R. Kishore, N.I. Kim, C. Prathap, S. Kumar, A comprehensive review of measurements and data analysis of laminar burning velocities for various fuel+air mixtures, Prog. Energy Combust. Sci. 68 (2018) 197–267, https://doi.org/10.1016/j.pecs.2018.05.003.
[18] F.N. Egolfopoulos, N. Hansen, Y. Ju, K. Kohse-Höinghaus, C.K. Law, F. Qi, Advances and challenges in laminar flame experiments and implications for combustion chemistry, Prog. Energy Combust. Sci. 43 (2014) 36–67, https://doi.org/10.1016/j.pecs.2014.04.004.
[19] D. Bjerketvedt, J.R. Bakke, K. Van Wingerden, Gas explosion handbook, J. Hazard Mater. 52 (1997) 1–150.
[20] O.R. Hansen, P. Hinze, D. Engel, S. Davis, Using computational fluid dynamics (CFD) for blast wave predictions, J. Loss Prev. Process. Ind. 23 (2010) 885–906, https://doi.org/10.1016/j.jlp.2010.07.005.
[21] D.G. Goodwin, H.K. Moffat, R.L. Speth, Cantera: an object-oriented software toolkit for chemical kinetics, thermodynamics, and transport processes, Version 2.4, https://doi.org/10.5281/zenodo.170284, 2017.
[22] G.P. Smith, D.M. Golden, M. Frenklach, N.W. Moriarty, B. Eiteneer, M. Goldenberg, C.T. Bowman, R.K. Hanson, S. Song, W.C.G. Jr, V.V. Lissianski, Z. Qin, GRI-MECH 3.0. http://combustion.berkeley.edu/gri-mech/version30/text30.html#cite, 1999. (Accessed 18 March 2018).
[23] M. Gao, M. Bi, L. Ye, Y. Li, H. Jiang, M. Yang, C. Yan, W. Gao, Suppression of hydrogen-air explosions by hydrofluorocarbons, Process Saf. Environ. Protect. 145 (2021) 378–387, https://doi.org/10.1016/j.psep.2020.08.036.
[24] MOZEES, MOZEES, mobil. Zero emiss. Energy syst. https://www.mozees.no/, 2017. (Accessed 20 August 2019).
[25] UCSD, Chemical-Kinetic Mechanisms for Combustion Applications", San Diego Mechanism Web Page, Mechanical and Aerospace Engineering (Combustion Research), University of California at San Diego, San Diego Mech, 2016. http://combustion.ucsd.edu.
[26] P.A. Glaude, W.J. Pitz, M.J. Thomson, Chemical kinetic modeling of dimethyl carbonate in an opposed-flow diffusion flame, Proc. Combust. Inst. 30 (2005) 1111–1118, https://doi.org/10.1016/j.proci.2004.08.096.
[27] W. Sun, B. Yang, N. Hansen, C.K. Westbrook, F. Zhang, G. Wang, K. Moshammer, C. K. Law, An experimental and kinetic modeling study on dimethyl carbonate (DMC) pyrolysis and combustion, Combust. Flame 164 (2016) 224–238, https://doi.org/10.1016/j.combustflame.2015.11.019.
[28] M. Henriksen, K. Vaagsaether, A.V. Gaathaug, J. Lundberg, S. Forseth, D. Bjerketvedt, Laminar burning velocity measurements for an outwardly propagating flame of dimethyl carbonate and air mixtures, in: Proc. Ninth Int. Semin. Fire Explos. Hazards, St. Petersburg Polytechnic University Press, St. Petersburg, 2019, pp. 161–172, https://doi.org/10.18720/spbpu/2/k19-29.
[29] M. Henriksen, D. Bjerketvedt, K. Vaagsaether, A.V. Gaathaug, T. Skjold, P. Middha, Accidental hydrogen release in a gas chromatograph laboratory: a case study, Int. J. Hydrogen Energy 42 (2017) 7651–7656, https://doi.org/10.1016/j.ijhydene.2016.05.299.
[30] G.S. Settles, Schlieren and Shadowgraph Techniques: Visualizing Phenomena in Transparent Media, Springer, Berlin ; New York, 2001.
[31] M. Henriksen, A.V. Gaathaug, K. Vaagsaether, J. Lundberg, S. Forseth, D. Bjerketvedt, Laminar burning velocity of the dimethyl carbonate-air mixture formed by the Li-ion electrolyte solvent, Combust. Explos. Shock Waves 56 (2020) 383–393, https://doi.org/10.1134/S0010508220040024.
[32] J. Johnsplass, Lithium-ion Battery Safety, University of South-Eastern Norway, 2017.
[33] M. Kuznetsov, S. Kobelt, J. Grune, T. Jordan, Flammability limits and laminar flame speed of hydrogen–air mixtures at sub-atmospheric pressures, Int. J. Hydrogen Energy 37 (2012) 17580–17588, https://doi.org/10.1016/j.ijhydene.2012.05.049.
[34] G. Dayma, New insights into the peculiar behavior of laminar burning velocities of hydrogen–air flames according to pressure and equivalence ratio, Combust. Flame (2014) 7.
[35] Z.H. Wang, W.B. Weng, Y. He, Z.S. Li, K.F. Cen, Effect of H2/CO ratio and N2/CO2 dilution rate on laminar burning velocity of syngas investigated by direct measurement and simulation, Fuel 141 (2015) 285–292, https://doi.org/10.1016/j.fuel.2014.10.040.
[36] P. Zahedi, K. Yousefi, Effects of pressure and carbon dioxide, hydrogen and nitrogen concentration on laminar burning velocities and NO formation of methane-air mixtures, J. Mech. Sci. Technol. 28 (2014) 377–386, https://doi.org/10.1007/s12206-013-0970-5.
[37] M.E. Bardin, E.V. Ivanov, E.J.K. Nilsson, V.A. Vinokurov, A.A. Konnov, Laminar burning velocities of dimethyl carbonate with air, Energy Fuels 27 (2013) 5513–5517, https://doi.org/10.1021/ef401108a.
[38] S. de Persis, N. Chaumeix, Y. Fernandes, A. Bry, A. Comandini, Experimental and theoretical determination of DMC/air flame velocities, in: 11th Int. Conf. Chem. Kinet., Orleans, 2019. Poster, https://icck2019.sciencesconf.org/data/pages/ICCK_Proc_final.pdf. (Accessed 13 August 2019).
[39] G. Rozenchan, D.L. Zhu, C.K. Law, S.D. Tse, Outward propagation, burning velocities, and chemical effects of methane flames up to 60 ATM, Proc. Combust. Inst. 29 (2002) 1461–1470, https://doi.org/10.1016/S1540-7489(02)80179-1.

[40] T. Boushaki, Y. Dhué, L. Selle, B. Ferret, T. Poinsot, Effects of hydrogen and steam addition on laminar burning velocity of methane–air premixed flame: experimental and numerical analysis, Int. J. Hydrogen Energy 37 (2012) 9412–9422, https://doi.org/10.1016/j.ijhydene.2012.03.037.

[41] I.C. McLean, D.B. Smith, S.C. Taylor, The use of carbon monoxide/hydrogen burning velocities to examine the rate of the CO+OH reaction, Symp. Int. Combust. 25 (1994) 749–757, https://doi.org/10.1016/S0082-0784(06)80707-1.

[42] H. Yu, W. Han, J. Santner, X. Gou, C.H. Sohn, Y. Ju, Z. Chen, Radiation-induced uncertainty in laminar flame speed measured from propagating spherical flames, Combust. Flame 161 (2014) 2815–2824, https://doi.org/10.1016/j.combustflame.2014.05.012.

[43] E.J.K. Nilsson, A. van Sprang, J. Larfeldt, A.A. Konnov, The comparative and combined effects of hydrogen addition on the laminar burning velocities of methane and its blends with ethane and propane, Fuel 189 (2017) 369–376, https://doi.org/10.1016/j.fuel.2016.10.103.

[44] O.K. Sommersel, D. Bjerketvedt, K. Vaagsaether, T.K. Fannelop, Experiments with release and ignition of hydrogen gas in a 3m long channel, Int. J. Hydrogen Energy 34 (2009) 5869–5874, https://doi.org/10.1016/j.ijhydene.2009.02.058.

[45] C.K. Law, Combustion Physics, Cambridge University Press, Cambridge ; New York, 2006.